InSAR Phase Unwrapping Based on Square-Root Cubature Kalman Filter

Xiaomei Luo, Hongtao Li, Zhilong Dong, and Shengqi Zhu

***Abstract*—In this article, we propose a novel phase unwrapping method termed the square-root cubature Kalman filter phase unwrapping (SCKFPU) method. Specifically, as the system model of the interferometric synthetic aperture (InSAR) phase unwrapping can be formulated as the discrete Markovian jump system for tracking a maneuvering target, a phase unwrapping method is proposed by combining the SCKF algorithm with a phase gradient estimator. Moreover, we design a phase quality estimate function, and present an optimal path-following strategy. The strategy ensures that the SCKFPU method simultaneously performs noise suppression and unwraps InSAR images along the pixels with high-reliance to the pixels with low-reliance. Simulation results based on synthetic data, true InSAR data, and measured (real) InSAR data show that the proposed InSAR phase unwrapping method can achieve better performance compared with other existing phase unwrapping methods.**

***Index Terms*—Optimal path-following strategy, phase quality estimate function, phase unwrapping, quality map, square-root cubature Kalman filter phase unwrapping (SCKFPU) method.**

I. Introduction

INTERFEROMETRIC synthetic aperture (InSAR) has been widely used in many applications, such as creating digital elevation models (DEMs) and monitoring surface deformation [1]. Two stages are needed in the standard processing procedure of differential InSAR data. In the first stage, data are handled by three steps, including filtering, coregistering, and flat-earth phase removing, whereas in the second stage, data are processed by two steps-phase filtering and phase unwrapping. Phase unwrapping is a key step to obtaining not only terrain height, but also displacement information.

There are two common approaches to InSAR phase unwrapping, one of which belongs to path-following methods and the other consists of minimum norm methods [2]. The branch-cut method is a very representative path-following method [3]. Although simple and fast, it can cause error propagation when larger noise values and more residual points exist in an image. Numerous improved path-following methods [4]-[8] have been proposed to overcome this weakness. One typical minimum norm method is the weighted least-squares phase unwrapping method [9]–[11]. Another typical minimum norm method is the network flow method [12]. Although interferometric phase fringes of the true phase are well consistent with those of the rewrapped phase, the slow unwrapping velocity and the requirement of high-performance computers are the drawbacks of this method.

Interferometric coherence is a very important parameter, which has plenty of InSAR application areas [13]–[15]. Srivastava *et al.* [13] exploited the interferometric coherence to map forest density, which suggests coherence is a parameter completely different from SAR backscatter and can provide valuable information. Luca *et al.* [14] jointly used the intensity and coherence to detect floodwater in urban and agricultural areas, which causes a considerable reduction of classification errors due to only considering intensity data. Kuma *et al.* [15] analyzed the Sentinel-1 interferometric coherence to mowing events on grasslands and concluded that afternoon acquisitions and steeper incidence angles are more useful in the context of this study. In this article, we will exploit the interferometric coherence to design a new phase estimate function, which helps select the unwrapping path and then guides the designed unwrapping method to work optimally.

InSAR phase unwrapping is a complex nonlinear optimization problem, which is extremely difficult to solve [16], [17]. Recently, there are some works studying the unwrapping problem based on nonlinear tracking filters in the Bayesian filter framework under the Gaussian domain [18]. Loffeld *et al.* [19] proposed the extended Kalman filter (EKF) phase unwrapping (EKFPU) method based on an EKF using a sequential path-following strategy. However, this method is not satisfactory especially for the pixels with bad quality maps. Martinez and Espla [20] proposed the particle filter (PF) phase unwrapping method based on a PF. Due to the particles introduced, the computational complexity of [20] is too high. Xie [21] proposed the unscented Kalman filter (UKF) phase unwrapping (UKFPU) method, an improved one which uses a UKF guided by an optimal path-following strategy. Liu *et al.* [22] proposed the cubature Kalman filter (CKF) phase unwrapping (CKFPU) method. Compared with other nonlinear tracking filters, CKFs are often capable of better tracking a maneuvering target due

Manuscript received June 21, 2020; accepted August 3, 2020. Date of publication August 11, 2020; date of current version August 24, 2020. This work was supported by the National Nature Science Fund of China (NSFC) under Grant 61661029 and in part by the Dr. Start-up Funding under Grant 06301229. The work of Z. Dong was supported by the NSFC under Grant 11801433. *(Corresponding author: Xiaomei Luo.)*

Xiaomei Luo is with the Department of Electronic Information Engineering, Nanchang University, Nanchang 330031, China, and also with the School of Economics and Finance, Xi'an Jiaotong University, Xi'an 710017, China (e-mail: xxxmluo@126.com).

Hongtao Li is with the Department of Electronic Information Engineering, Nanchang University, Nanchang 330031, China (e-mail: 2504121747@qq.com).

Zhilong Dong is with the School of Economics and Finance, Xi'an Jiaotong University, Xi'an 710017, China (e-mail: zldong@xjtu.edu.cn).

Shengqi Zhu is with the National Laboratory of Radar Signal Processing, Xidian University, Xi'an 710017, China (e-mail: sqzhu@xidian.edu.cn).

Digital Object Identifier 10.1109/JSTARS.2020.3015739

to the third-degree spherical-radial cubature rule applied to deal with multidimensional integrals [23]. Thereby, the CKFPU method can achieve a better performance in InSAR phase unwrapping. However, the phase unwrapping performance is not satisfying as the selected parameter may prevent the CKFPU method from running continuously.

In this article, we present a novel phase unwrapping method based on a square-root cubature Kalman filter (SCKF). The main contributions are as follows.

First, we propose a phase unwrapping method termed the SCKFPU method. Although simple, EKFs and UKFs cannot meet the demands from many complex tracing applications. It is well known that preserving symmetry and positive definiteness of an error covariance matrix in each cycle is very important for most tracking algorithms. Because of the errors introduced by finite word-length effects and Cholesky decomposition directly applied to the error covariance matrix, CKFs [23], [24] often lose these two basic properties, which may stop the unwrapping process. In other words, the CKFPU method is not able to select the parameter freely to continuously unwrap an InSAR image and thus may not yield the correct result [22]. On the other hand, SCKFs can make the algorithm work continuously by using least-squares method for the Kalman gain and orthogonal matrix-triangularization (QR) decomposition for the error covariance matrix. In this article, we exploit an SCKF to design the SCKFPU phase unwrapping method which overcomes the shortcomings of a CKF, and thus, is more suitable for the complex InSAR phase unwrapping problem.

Second, a phase estimate function is designed to help select the unwrapping path and guide the SCKFPU method to work optimally. The SCKFPU method on a sequential path-following strategy can well tackle pixels when an image is noise-free. However, when an image is noisy, the unwrapping performance is degraded due to error propagation. Thereby, the optimal following path is selected by minimizing the designed phase estimate function, which ensures the proposed method simultaneously performs noise suppression and unwraps InSAR images along the pixels with high-reliance (the smaller values of the phase estimate function) to the pixels with low-reliance (the larger values of the phase estimate function). In this way, the SCKFPU method can achieve a better unwrapping performance compared with the one guided only by the coherence or by the phase estimate function in [21], which can be proved by our simulations.

The rest of this article is organized as follows. In Section II, local phase-gradient estimation is described. The SCKFPU method is presented in Section III. Extensive simulations including synthetic data, true InSAR data, and measured (real) InSAR data are illustrated in Section IV. Finally, Section V concludes this article.

II. Local Phase-Gradient Estimation

A. Complex InSAR Phase Model

For a complex noisy SAR interferogram, we can describe it in polar form as

$$\tilde{z}(x,y) = \tilde{a}(x,y)\exp(I\tilde{\phi}(x,y)) \qquad x = 1,\ldots,N,\ y = 1,\ldots,M \tag{1}$$

where $I = \sqrt{-1}$; x and y represent row and column indexes, respectively; M and N represent the lengths of row and column of the complex SAR interferogram, respectively; and $\tilde{a}(x,y)$ and $\tilde{\phi}(x,y)$ are the complex amplitude and the interferometric phase modulo 2π mapped of the complex signal point at pixel (x,y).

In (1), $\tilde{\phi}(x,y)$ can be expressed by [25]

$$\begin{aligned}\tilde{\phi}(x,y) &= [\phi(x,y) + e_\phi(x,y)]_{|2\pi} \\ &= [\phi(x,y) + e_\phi(x,y)_{|2\pi}]_{|2\pi} \\ &= [\phi(x,y) + \tilde{e}_\phi(x,y)]_{|2\pi}\end{aligned} \tag{2}$$

where $\phi(x,y)$ is the true unambiguous phase at pixel (x,y); $e_\phi(x,y)$ is the true phase error at pixel (x,y); and $\tilde{e}_\phi(x,y)$ is the mapped phase error at pixel (x,y), which satisfies $\tilde{e}_\phi(x,y) = [\tilde{e}_\phi(x,y) + 2\pi n]_{|2\pi} = e_\phi(x,y)_{|2\pi}, n \in \mathbb{Z}$.

Substituting (2) into (1), we have

$$\begin{aligned}&\tilde{z}(x,y) = \tilde{a}(x,y)\left[\exp(I(\phi(x,y) + \tilde{e}_\phi(x,y)))\right] \\ &\approx \tilde{a}(x,y)\left[\exp(I\phi(x,y)) + I\exp(\tilde{e}_\phi(x,y))\exp(I\phi(x,y))\right] \\ &= \tilde{a}(x,y)\left[\exp(I\phi(x,y)) + v(x,y)\right]\end{aligned} \tag{3}$$

where the first equality is due to the invariability of $\exp(\cdot)$ for the phase $\phi(x,y) + \tilde{e}_\phi(x,y)$ and the mapped phase $\tilde{\phi}(x,y)$; the approximation is due to the first-order Taylor of $\tilde{e}_\phi(x,y)$, and $v(x,y)$ denotes the complex additive Gaussian noise at pixel (x,y), with zero mean and variable variance varying with its coherence [24].

From (2), the phase unwrapping problem, recovering $\phi(x,y)$ from $\tilde{\phi}(x,y)$, is a complex nonconvex integer optimization problem [26] that is difficult to solve. In order to develop our unwrapping method, we will establish the complex InSAR phase model in the sequel.

Assume that there is a single sinusoidal frequency set $\{\hat{f}_x, \hat{f}_y\}$ in a local interferogram observation window, where $\hat{f}_x$ and $\hat{f}_y$ are the row and column mean fringe frequencies, respectively. Also assume that the true unambiguous phase and the interferometric phase at pixel $\{x_0, y_0\}$ are $\phi(x_0,y_0)$ and $\tilde{\phi}(x_0,y_0)$, respectively. Thereby, the true unambiguous phase at pixel $\{x,y\}$ can be obtained by [27]

$$\begin{aligned}\phi(x,y) &= \phi(x_0,y_0) + \int_{y_0}^{y}\int_{x_0}^{x}\nabla\phi(x,y)d\boldsymbol{x}d\boldsymbol{y} \\ &= \tilde{\phi}(x_0,y_0) + \int_{x_0}^{x}\frac{\partial\phi(x,y)}{\partial x}dx + \int_{y_0}^{y}\frac{\partial\phi(x,y)}{\partial y}dy \\ &= \tilde{\phi}(x_0,y_0) + 2\pi\int_{x_0}^{x}\hat{f}_x dx + 2\pi\int_{y_0}^{y}\hat{f}_y dy.\end{aligned} \tag{4}$$

Here, $d\boldsymbol{x} = \vec{i}dx$ and $d\boldsymbol{y} = \vec{j}dy$, where $\vec{i}$ and $\vec{j}$ are the unit vector in x-direction and y-direction, respectively; ∇ is the gradient operator, defined as $\nabla = \frac{\partial}{\partial x}\vec{i} + \frac{\partial}{\partial y}\vec{j}$. The second equality is due to $\phi(x_0,y_0) = \tilde{\phi}(x_0,y_0)$.

Assume that the noisy interferogram is not undersampled. $\hat{f}_x$ and $\hat{f}_y$ can be approximated as

$$\hat{f}_x \approx f_x,\ \hat{f}_y \approx f_y \tag{5}$$

where f_x and f_y are the row and column mean frequencies in a local unwrapped image, respectively.

Accordingly, (4) can be closely approximated as

$$\phi(x,y) \approx \tilde{\phi}(x_0,y_0) + 2\pi \int_{x_0}^{x} f_x dx + 2\pi \int_{y_0}^{y} f_y dy = 2\pi f_x x + 2\pi f_y y. \quad (6)$$

Substituting (6) into (3) with a normalized form, we establish the complex InSAR phase model as

$$\tilde{z}(x,y) = \exp\{I2\pi(f_x x + f_y y)\} + v(x,y). \quad (7)$$

In the following section, we will establish the observation function from (7) and then propose the SCKFPU method.

B. Local Phase-Gradient Estimation

There are many methods to estimate the local phase slope, such as Madsen′s correlation Doppler estimator [28]. In what follows, we will estimate the phase gradient of the wrapped phase by maximum likelihood (ML) estimator combined with linear chirp-z transform (CZT). Specifically, the central frequencies of each local block InSAR image are roughly estimated by ML estimation, followed by refined estimation using CZT.

Extract the local region with the size of $B_n \times B_m$ that satisfies the independent identical distribution. The rough estimation of the row and column frequencies of the central pixel (k,h) can be mathematically represented as

$$\{\begin{matrix}\bar{f}_x \\ \bar{f}_y\end{matrix}\} = \arg\max_{\{f_x,f_y\}} \left\{ \sum_{x,y} \left| \tilde{z}(x,y)\exp\{-I2\pi(f_x x + f_y y)\} \right| \right\}$$
$$k-(B_n-1)/2 \le x \le k+(B_n-1)/2$$
$$h-(B_m-1)/2 \le y \le h+(B_m-1)/2 \quad (8)$$

where k and h are the row and column numbers of the central pixel in the local region, respectively.

Subsequently, the refined estimates $\tilde{f}_x$ and $\tilde{f}_y$ can be attained in three steps. First, we extract a local window centering at the rough estimates $\bar{f}_x$ and $\bar{f}_y$. Second, the data in the local window can be transformed into frequency domain by first-order CZT in the x-axis direction, followed by in the y-axis direction. Finally, the ML estimator is used to attain the refined estimates $\tilde{f}_x$ and $\tilde{f}_y$.

Cramer–Rao lower bound (CRLB) provides a lower bound for the second-order (mean-squared) error of any estimate method [30]. The CRLB values $c(\tilde{f}_x)$ and $c(\tilde{f}_y)$ of the local frequency estimates $\tilde{f}_x$ and $\tilde{f}_y$ are used to compute the estimate error variances of local phase gradient estimates, which can be represented as [31]

$$c(\tilde{f}_x) = \frac{6}{\gamma B_m B_n (B_m^2-1)} \quad (9)$$

$$c(\tilde{f}_y) = \frac{6}{\gamma B_m B_n (B_n^2-1)} \quad (10)$$

TABLE I
LOCAL PHASE-GRADIENT ESTIMATION

1: Local frequency estimation by the ML plus CZT method.
2: Cramer-Rao Lower Bound by (9) and (10) using local frequency estimates.
3: Local phase gradient estimation by (12).
4: Error variances of local phase gradient estimates by Eq. (13) and Eq. (14), respectively.

where γ is the correlation parameter of a local interferogram, which can be estimated using the following equation:

$$\gamma = \frac{\mathbb{E}(|\tilde{a}(x,y)|^2)}{2\mathbb{E}(|v(x,y)|^2)} \quad (11)$$

where $\mathbb{E}$ represents the statistics expectation.

And the phase-gradient estimation for pixel (x,y) in the local region with the central pixel (k,h) can be estimated as

$$\tilde{\delta}_\phi(x,y) = 2\pi\tilde{f}_x(x-k) + 2\pi\tilde{f}_y(y-h)$$
$$-(B_m-1)/2+k \le x \le (B_m-1)/2+k$$
$$-(B_n-1)/2+h \le y \le (B_n-1)/2+h. \quad (12)$$

Using (9), (10), and (12), the estimate error variances of local phase gradient estimates for pixel (x,y) in the x-axis and y-axis directions can be computed as

$$\sigma_x^2 = (2\pi)^2(x-k)^2 c(\tilde{f}_x) \quad (13)$$

$$\sigma_y^2 = (2\pi)^2(y-h)^2 c(\tilde{f}_y)$$
$$-(B_m-1)/2+k \le x \le (B_m-1)/2+k$$
$$-(B_n-1)/2+h \le y \le (B_n-1)/2+h. \quad (14)$$

The main steps of local phase-gradient estimation are given in Table I.

III. SCKFPU METHOD

In this section, we will design a phase unwrapping method based on the SCKF algorithm. The system model of InSAR phase unwrapping is establish, and then an SCKFPU method is proposed. Specifically, we propose an optimal phase estimate function and an optimal path selection strategy. Then, a novel phase unwrapping method is presented, which is based on the SCKF algorithm guided by this optimal path-following strategy.

A. System Model of InSAR Phase Unwrapping

The system model of InSAR phase unwrapping can be formulated as the discrete Markovian jump system (MJS) for tracking a maneuvering target [19]. Thereby, we can use the basic state function and observation function to describe the model, which are depicted in the sequel.

1) Basic State Function: Suppose that the true phases are stacked in a vector, and the basic state function of the unwrapped pixels can be represented as [19]

$$\phi(k+1) = \phi(k) + \vec{\delta}_\phi(k) + w(k) \quad (15)$$

where $\phi(k) \in \mathbb{R}$ is the basic state, representing the true unambiguous phase at pixel k; $\vec{\delta}_\phi(k) \in \mathbb{R}$ is the phase slope estimate of the true phase at pixel k; $w(k) \in \mathbb{R}$ is the corresponding estimate error of the true phase slope at pixel k, satisfying $\mathbb{E}[w(k)] = 0$, $Q_k = \mathbb{E}[w(k)w(j)^T] = \sigma_w^2 \delta(k,j)$, Q_k is the covariance function of the error of phase slope $\vec{\delta}_\phi(k)$, σ_w^2 is the corresponding variance, $\delta(k,j)$ is the discrete Dirac impulse, defined as

$$\delta(k,j) = \begin{cases} 1, \text{ if } k = j \\ 0, \text{ else} \end{cases} \tag{16}$$

where k and j are the pixel serial numbers.

2) Observation Function: Suppose that the complex measurement data are stacked in a vector, and the observation function of the true unambiguous phase normalized at pixel k usually can be represented as [19]

$$\begin{aligned} \mathbf{z}(k) &= \begin{bmatrix} \frac{\mathrm{Im}[\tilde{z}(k)]}{\tilde{a}(k)} \\ \frac{\mathrm{Re}[\tilde{z}(k)]}{\tilde{a}(k)} \end{bmatrix} = \begin{bmatrix} \sin(\phi(k)) \\ \cos(\phi(k)) \end{bmatrix} + \begin{bmatrix} v_1(k) \\ v_2(k) \end{bmatrix} \\ &= \mathbf{H}[\phi(k)] + \mathbf{v}(k) \end{aligned} \tag{17}$$

where $\mathbf{z}(k) \in \mathbb{R}^2$ is the normalized observation vector at pixel k; $\mathbf{H}(\cdot)$ denotes the observation function; $\mathbf{v}(k) \in \mathbb{R}^2$ represents the normalized observation noise at pixel k, satisfying $\mathbb{E}[\mathbf{v}(k)] = \mathbf{0}, \mathbf{R}_k = \mathbb{E}[\mathbf{v}(k)\mathbf{v}(j)^T] = \mathrm{diag}(\sigma_{\mathbf{v}}^2(k)\delta(k,j))$; and $v_1(k)$ and $v_2(k)$ are the errors of the real and imaginary parts of the normalized complex noise at pixel k, respectively.

B. SCKF Algorithm

Before designing the SCKFPU method, we introduce the SCKF algorithm for InSAR phase unwrapping [29]. The notations involved in the SCKF formulations are described as follows.

1) A general triangularization algorithm is denoted by $\mathbf{S} = \mathrm{Tria}(\mathbf{A})$, and $\mathbf{P} = \mathbf{A}\mathbf{A}' = \mathbf{S}\mathbf{S}'$, where $'$ is the conjugate transpose, where $\mathbf{P}$ is some semidefinite positive matrix, $\mathbf{A}$ is obtained by Cholesky factorization of $\mathbf{P}$, and $\mathbf{S}$ is obtained by QR decomposition of $\mathbf{A}$.
2) $S_{Q,k} \in \mathbb{R}$ and $\mathbf{S}_{\mathbf{R},k} \in \mathbb{R}^{2\times 2}$ are square-roots of covariance matrices $Q_k \in \mathbb{R}$ and $\mathbf{R}_k \in \mathbb{R}^{2\times 2}$ of the process and measurement noises, respectively.
3) Many recursive steps of the Bayesian filter are to compute Gaussian weighted integrals with the form nonlinear function $\times$ Gaussian density. The SCKF (CKF) algorithm exploits the third-degree spherical-radial cubature rule to deal with this kind of multidimensional integrals to obtain better numerical accuracy. $\xi_i \in \mathbb{R}, i = 1, 2, \ldots, m$ are the cubature points, which are generated from the spherical-radial cubature rule used by the SCKF (CKF) algorithm. Mathematically, this algorithm solves lots of approximate equations similar to

$$\int_{\mathbb{R}^n} f(\mathbf{x}) \mathcal{N}(\mathbf{x}; \mathbf{0}, \mathbf{I}) \approx \sum_{i=1}^{m} \omega_i f(\xi_i) \tag{18}$$

where $f(\mathbf{x})$ is a nonlinear function; $\mathcal{N}(\mathbf{x}; \mathbf{0}, \mathbf{I})$ is the Gaussian probability function of $\mathbf{x}$ with mean vector $\mathbf{0}$ and covariance matrix $\mathbf{I}$; ξ_i is the cubature point and ω_i is the corresponding weight.

SCKF Algorithm

State prediction at pixel k: true phase prediction at pixel k.

1) Evaluate the cubature points $i = 1, \ldots, m$

$$x_{i,j} = S_{j|j}\xi_i + \hat{x}_{j|j} \tag{19}$$

where m is the number of the cubature points, $j \in \overset{o}{\mathcal{U}}(k-1)$ and $\overset{o}{\mathcal{U}}(k-1)$ denotes the set consisting of the adjacent pixels of the unwrapping pixel k; $x_{i,j} \in \mathbb{R}$ is the state related to the cubature point ξ_i at the pixel j; $S_{j|j} \in \mathbb{R}$, computed by (36), denotes the square-root factor of the error covariance at pixel j; $\hat{x}_{j|j} \in \mathbb{R}$, computed by (35), denotes the updated state at pixel j; n_x, set as 1, denotes the number of unwrapping pixels at one time; $m = 2n_x$ denotes the number of cubature points; and the cubature points $\xi_i = \sqrt{m/2}u^{(i)}$, where $u^{(i)} \in \mathbb{R}$ belongs to the following set of points:

$$u(k-1) = \{1 \ -1\}. \tag{20}$$

2) Evaluate the propagated cubature points $i = 1, \ldots, m$

$$x^*_{i,k|j} = x_{i,j} + \vec{\delta}_j \tag{21}$$

where $j \in \overset{o}{\mathcal{U}}(k-1)$; $x^*_{i,k|j}$ is the predicted state related to the cubature point ξ_i and the unwrapping pixel k from pixel j; $x_{i,j}$ is the state related to cubature point ξ_i and pixel j; $\vec{\delta}_j$ denotes the phase-gradient estimation for pixel j, which is computed by (12).

3) Estimate the predicted state $\hat{x}_{k|\overset{o}{\mathcal{U}}(k-1)} \in \mathbb{R}$ at pixel k

$$\hat{x}_{k|\overset{o}{\mathcal{U}}(k-1)} = \sum_{j=1}^{K} \left[\bar{\mathbf{W}}_j \frac{1}{m} \sum_{i=1}^{m} x^*_{i,k|j} \right] \tag{22}$$

where $j \in \overset{o}{\mathcal{U}}(k-1)$ and K denotes the number in the set $\overset{o}{\mathcal{U}}(k-1)$; $\bar{\mathbf{W}}_j$ is the weight for j

$$\bar{\mathbf{W}}_j = \frac{\mathrm{SNR}_j \mathrm{Up}_j}{\sum_{j=1}^{K} \mathrm{SNR}_j \mathrm{Up}_j} \tag{23}$$

where SNR_j denotes the signal-to-noise ratio (SNR) for pixel j and Up_j denotes the unwrapped indicator for pixel j, which is defined as

$$\mathrm{Up}_j = \begin{cases} 1, \text{ wrapped} \\ 0, \text{ unwrapped.} \end{cases} \tag{24}$$

4) Estimate the square-root factor of the predicted error covariance $S_{k|\overset{o}{\mathcal{U}}(k-1)} \in \mathbb{R}$ at pixel k

$$S_{k|\overset{o}{\mathcal{U}}(k-1)} = \sum_{j=1}^{K} \bar{\mathbf{W}}_j \mathrm{Tria}\left(\left[\boldsymbol{\chi}^*_{k|j}, S_{Qj} \right] \right) \tag{25}$$

where $j \in \overset{o}{\mathcal{U}}(k-1)$ denotes a square-root factor of Q_j such that $Q_j = S_{Qj}S'_{Qj}$; Q_j denotes the estimated error

variance at pixel j computed by (13) or (14); and $\boldsymbol{\chi}^*_{k|j}$ is the weighted, centered predicted state matrix for pixel j

$$\boldsymbol{\chi}^*_{k|j}=\frac{1}{\sqrt{m}}\left[x^*_{1,k|j}-\hat{x}_{k|\overset{o}{\mathcal{U}}(k-1)},\ x^*_{2,k|j}-\hat{x}_{k|\overset{o}{\mathcal{U}}(k-1)}\right.$$
$$\left.\ldots,\ x^*_{m,k|j}-\hat{x}_{k|\overset{o}{\mathcal{U}}(k-1)}\right]. \tag{26}$$

State update at pixel k: true phase update at pixel k.

1) Evaluate the cubature points $i=1,\ldots,m$

$$x_{i,k|\overset{o}{\mathcal{U}}(k-1)}=S_{k|\overset{o}{\mathcal{U}}(k-1)}\xi_i+\hat{x}_{k|\overset{o}{\mathcal{U}}(k-1)} \tag{27}$$

where $x_{i,k|\overset{o}{\mathcal{U}}(k-1)}\in\mathbb{R}$ is the repredicted state related to ξ_i.

2) Evaluate the propagated cubature points $i=1,\ldots,m$

$$\mathbf{z}_{i,k|\overset{o}{\mathcal{U}}(k-1)}=\mathbf{H}\left(x_{i,k|\overset{o}{\mathcal{U}}(k-1)}\right)=\begin{bmatrix}\sin\left(x_{i,k|\overset{o}{\mathcal{U}}(k-1)}\right)\\ \cos\left(x_{i,k|\overset{o}{\mathcal{U}}(k-1)}\right)\end{bmatrix} \tag{28}$$

where $\mathbf{z}_{i,k|\overset{o}{\mathcal{U}}(k-1)}\in\mathbb{R}^2$ is the predicted measurement related to ξ_i.

3) Estimate the predicted measurement $\hat{\mathbf{z}}_{k|\overset{o}{\mathcal{U}}(k-1)}\in\mathbb{R}^2$ at pixel k

$$\hat{\mathbf{z}}_{k|\overset{o}{\mathcal{U}}(k-1)}=\frac{1}{m}\sum_{i=1}^{m}\mathbf{z}_{i,k|\overset{o}{\mathcal{U}}(k-1)}. \tag{29}$$

4) Estimate the square-root of the innovation covariance matrix $\mathbf{S}_{zz,k|\overset{o}{\mathcal{U}}(k-1)}\in\mathbb{R}^2$ at pixel k

$$\mathbf{S}_{zz,k|\overset{o}{\mathcal{U}}(k-1)}=\text{Tria}\left(\left[\mathcal{Z}_{k|\overset{o}{\mathcal{U}}(k-1)},\quad \mathbf{S}_{\mathbf{R},k}\right]\right) \tag{30}$$

where $\mathbf{S}_{\mathbf{R},k}\in\mathbb{R}^{2\times2}$ denotes a square-root factor of $\mathbf{R}_k\in\mathbb{R}^{2\times2}$ such that $\mathbf{R}_k=\mathbf{S}_{\mathbf{R},k}\mathbf{S}'_{\mathbf{R},k}$ and $\mathcal{Z}_{k|\overset{o}{\mathcal{U}}(k-1)}$ is the weighted, centered predicted observation matrix

$$\mathcal{Z}_{k|\overset{o}{\mathcal{U}}(k-1)}=\frac{1}{\sqrt{m}}\left[\mathbf{z}_{1,k|\overset{o}{\mathcal{U}}(k-1)}-\hat{\mathbf{z}}_{k|\overset{o}{\mathcal{U}}(k-1)},\ \mathbf{z}_{2,k|\overset{o}{\mathcal{U}}(k-1)}\right.$$
$$\left.-\hat{\mathbf{z}}_{k|\overset{o}{\mathcal{U}}(k-1)},\ldots,\ \mathbf{z}_{m,k|\overset{o}{\mathcal{U}}(k-1)}-\hat{\mathbf{z}}_{k|\overset{o}{\mathcal{U}}(k-1)}\right]. \tag{31}$$

5) Estimate the cross-covariance matrix $\mathbf{P}_{xz,k|\overset{o}{\mathcal{U}}(k-1)}\in\mathbb{R}^{1\times2}$

$$\mathbf{P}_{xz,k|\overset{o}{\mathcal{U}}(k-1)}=\boldsymbol{\chi}_{k|\overset{o}{\mathcal{U}}(k-1)}\mathcal{Z}'_{k|\overset{o}{\mathcal{U}}(k-1)} \tag{32}$$

where $\boldsymbol{\chi}_{k|\overset{o}{\mathcal{U}}(k-1)}$ is the weighted, centered repredicted observation matrix

$$\boldsymbol{\chi}_{k|\overset{o}{\mathcal{U}}(k-1)}=\frac{1}{\sqrt{m}}\left[x_{1,k|\overset{o}{\mathcal{U}}(k-1)}-\hat{x}_{k|\overset{o}{\mathcal{U}}(k-1)},\ x_{2,k|\overset{o}{\mathcal{U}}(k-1)}\right.$$
$$\left.-\hat{x}_{k|\overset{o}{\mathcal{U}}(k-1)},\ldots,\ x_{m,k|\overset{o}{\mathcal{U}}(k-1)}-\hat{x}_{k|\overset{o}{\mathcal{U}}(k-1)}\right]. \tag{33}$$

6) Estimate the Kalman gain $\mathbf{W}_k\in\mathbb{R}^{1\times2}$

$$\mathbf{W}_k=\left(\mathbf{P}_{xz,k|\overset{o}{\mathcal{U}}(k-1)}/\mathbf{S}'_{zz,k|\overset{o}{\mathcal{U}}(k-1)}\right)/\mathbf{S}_{zz,k|\overset{o}{\mathcal{U}}(k-1)}. \tag{34}$$

7) Estimate the updated state $\hat{x}_{k|k}\in\mathbb{R}$

$$\hat{x}_{k|k}=\hat{x}_{k|\overset{o}{\mathcal{U}}(k-1)}+\mathbf{W}_k(\mathbf{z}_k-\hat{\mathbf{z}}_{k|\overset{o}{\mathcal{U}}(k-1)}) \tag{35}$$

where $\hat{x}_{k|\overset{o}{\mathcal{U}}(k-1)}$, $\hat{\mathbf{z}}_{k|\overset{o}{\mathcal{U}}(k-1)}$ and $\mathbf{W}_k$ can be computed by (22), (29), and (34), respectively.

8) Estimate the square-root factor of the error covariance $S_{k|k}\in\mathbb{R}$ at pixel k

$$S_{k|k}=\text{Tria}\left(\left[\boldsymbol{\chi}_{k|\overset{o}{\mathcal{U}}(k-1)}-\mathbf{W}_k\mathcal{Z}_{k|\overset{o}{\mathcal{U}}(k-1)},\mathbf{W}_k\mathbf{S}_{\mathbf{R},k}\right]\right) \tag{36}$$

where $\mathcal{Z}_{k|\overset{o}{\mathcal{U}}(k-1)}$, $\boldsymbol{\chi}_{k|\overset{o}{\mathcal{U}}(k-1)}$, and $\mathbf{W}_k$ can be computed by (31), (33), and (34), respectively.

C. Optimal Path-Following Strategy and Main Steps of the SCKFPU Method

A direct application of the SCKFPU method to unwrap the InSAR phase on a sequential path-following strategy works very well in some cases. However, it is likely to cause error propagation, especially for the pixels with low-quality maps. Thereby, we design a strategy that optimally selects the path to guide the SCKFPU method to unwrap InSAR phases.

Considering the correlation between the pixels and error estimation of the phase gradient of each local pixel, the phase estimate function is designed based on the coherence coefficient and the phase derivative variance [2] of a wrapped phase image. Just as the coherence coefficient is a quality map, so is the phase derivative variance that is defined as the statistical variance of the phase derivative. Mathematically, the phase estimate function is designed as

$$q(x,y)=\text{der}(x,y)/[\text{coh}(x,y)]^r \tag{37}$$

where $q(x,y)$ is referred to as the value of phase quality estimate function of a wrapped phase image at pixel (x,y), $\text{coh}(x,y)$ is the coherence coefficient at pixel (x,y), and r is the adjustable weight, reflecting the effect of the coherence on the phase quality estimate function. The larger the value of the coherence, the smaller the value of $q(x,y)$. The selection of r is heavily dependent on the image itself. It is worthwhile to preset the weight r by trial to adjust the phase quality estimate function. The range $1.1\le r\le 2.3$ is acceptable for trying. $\text{der}(x,y)$ is the phase derivative variance at pixel (x,y), which is computed as

$$\text{der}(x,y)=\frac{\sqrt{\sum\left(\nabla^1_{i,j}-\overline{\nabla^1}_{x,y}\right)^2}+\sqrt{\sum\left(\nabla^2_{i,j}-\overline{\nabla^2}_{x,y}\right)^2}}{K^2} \tag{38}$$

where the indexes (i,j) range over the $K\times K$ window centered at pixel (x,y) for each sum. The terms $\nabla^1_{i,j}$ and $\nabla^2_{i,j}$ are the partial derivatives of the phase (i.e., the wrapped phase

differences). The terms $\overline{\nabla^1}_{x,y}$ and $\overline{\nabla^2}_{x,y}$ are the averages of these partial derivatives in the $K \times K$ window.

In this article, we select the optimal path by minimizing phase quality estimate function (37), along which the SCKFPU method works. The optimal path-following strategy ensures that the SCKFPU method simultaneously reduces the noise and unwraps the phase along the pixels with high-reliance to the pixels with low-reliance. The main steps of the SCKFPU method are as follows.

Step 1. *Initialization:* A pixel with the smallest phase quality estimate function is selected as the beginning pixel. Then, the four adjacent pixels of the beginning pixel are marked as waiting pixels.

Step 2. The waiting pixel with the smallest phase quality estimate function is marked as the current pixel and is unwrapped using the SCKFPU method. Then, the wrapped pixels among four adjacent pixels of the current pixel are marked as waiting pixels. Finally, the current pixel is removed from the set of waiting pixels.

Step 3. If there are waiting pixels to be unwrapped, return to Step 2; otherwise, end.

IV. Numerical Experiments

A. Evaluating Metrics

We will use several metrics to evaluate the performance of the proposed SCKFPU method. One commonly used metric is the residue count, which is defined as the number of the nonzero sum of the wrapped gradients in each 2×2 region in an InSAR phase [32]. Usually, a low-residue count indicates a good phase unwrapping result. Another metric used to assess the performance of InSAR phase unwrapping methods is the mean-square error (MSE), which has two definitions, one for a wrapped phase image and the other for an unwrapped image. The MSE for a wrapped phase is defined as [33]

$$\mathbf{MSE} = \mathbb{E}\left[|\arg\exp\left(I\hat{\varphi} - I\varphi_{\text{ideal}}\right)|^2\right] \tag{39}$$

where φ_{ideal} is the true InSAR phase and $\hat{\varphi}$ is the estimated wrapped phase. The MSE for an unwrapped phase is defined as [34]

$$\mathbf{MSE} = \mathbb{E}\left[|\hat{\Phi} - \Phi_{\text{ideal}}|^2\right] \tag{40}$$

where Φ_{ideal} is the true absolute phase and $\hat{\Phi}$ is the unwrapped phase. The smaller the MSE, the better the performance of InSAR phase unwrapping.

In addition, other indexes are used to evaluate the performance of InSAR phase unwrapping methods. One is the SNR, which is defined as the ratio of the average power of the noise-free part to that of the noise part in the unwrapped image. The larger the SNR, the better the noise reduction.

Another index is the number of errors larger than π (NELP) [36] and the other difference phase. From the estimated phase $\{\hat{\Phi}_i, i = 1, \ldots, N_s\}$ of the phase $\{\Phi_i, i = 1, \ldots, N_s\}$ without noise, define the set of image pixels with error no larger than π, i.e., $I_s := \{i : |\hat{\Phi}_i - \Phi_i| \leq \pi, i = 1, \ldots, N_s\}$, and define NELP as

$$\text{NELP} := N_s - |I_s|. \tag{41}$$

The lower the NELP, the better the discontinuity preservation.

Three definitions of the difference phase are used to evaluate the performance of InSAR phase unwrapping methods. The first is the difference phase, which is defined as the difference between the unwrapped phase and the original true phase. The second is the difference interferometric phase, which is defined as the difference between the rewrapped phase and the original true wrapped phase. And the third is the wrapped difference phase, which is defined as the wrapped difference between the original wrapped phase and the unwrapped phase [35]. The first two definitions are applied to original true data, whereas the third to measured data. For the first two definitions, the less the noises and residuals, the better the unwrapping performance. For the third, the more homogeneous the distribution of residuals and noises, the better the unwrapping performance. Moreover, the less the fringes, the better the unwrapping performance.

TABLE II
MSE Values for Unwrapped Phases

Methods	MSE(rad^2)
EKFPU	17.2209
UKFPU	0.3772
CKFPU	0.0150
SCKFPU	$5.3296e-04$

B. Synthetic Data

In the first scenario, generate a phase by using the "peaks" function in MATLAB, xy_phase $= a \cdot$ peaks(N), where $a = 10$, $N = 259$. We use the methods EKFPU [19], UKFPU [21], CKFPU [22], and the proposed method SCKFPU on a sequential path-following strategy to unwrap the wrapped image of the "peaks" image. The value of the adjustable weight r is set as 1.8. The MSE values for the unwrapped phases are listed in Table II.

The wrapped phases, the unwrapped phases, and the difference phases are shown in Fig. 1 , respectively. It is obvious that the SCKFPU method is the best whereas the EKFPU method is the worst of all the phase unwrapping methods. From Table II and Fig. 1, the SCKFPU method has not only the best unwrapped image, but also the smallest MSE value and the "clearest" difference image. Although the EKFPU method is simple, its unwrapping performance is the worst due to the low sampling frequency and the complex nonlinearity of the phase unwrapping problem.

Because the unwrapped images using the CKFPU method and SCKFPU method appear similar from Fig. 1, we compare their performance by unwrapping the same dataset with reduced size. Suppose that $N = 257$, and the rewrapped results using the CKFPU and SCKFPU on a sequential path-following strategy are shown in Fig. 2.

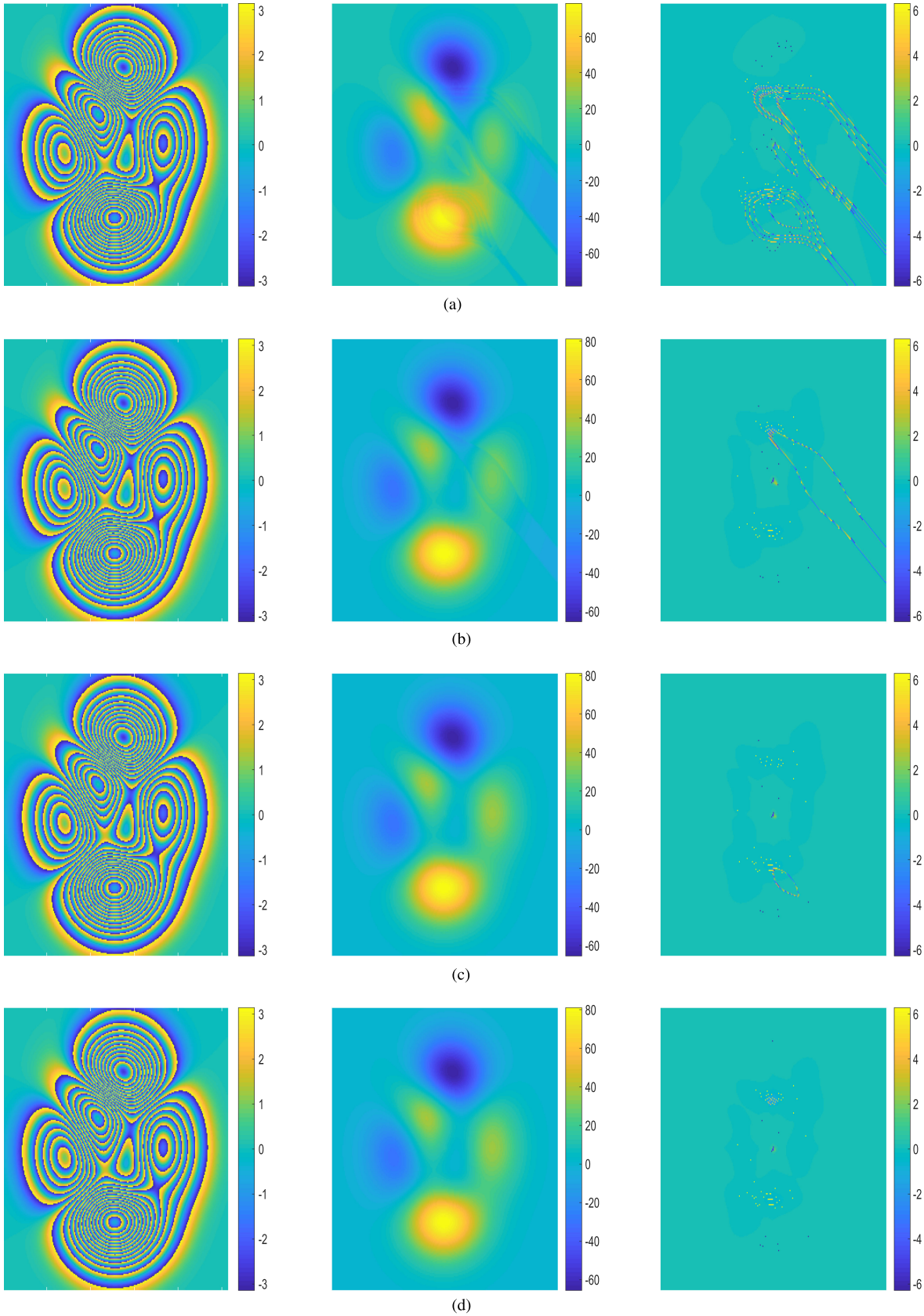

Fig. 1. Unwrapping results. Left: wrapped phases; center: unwrapped phases; right: difference phases.

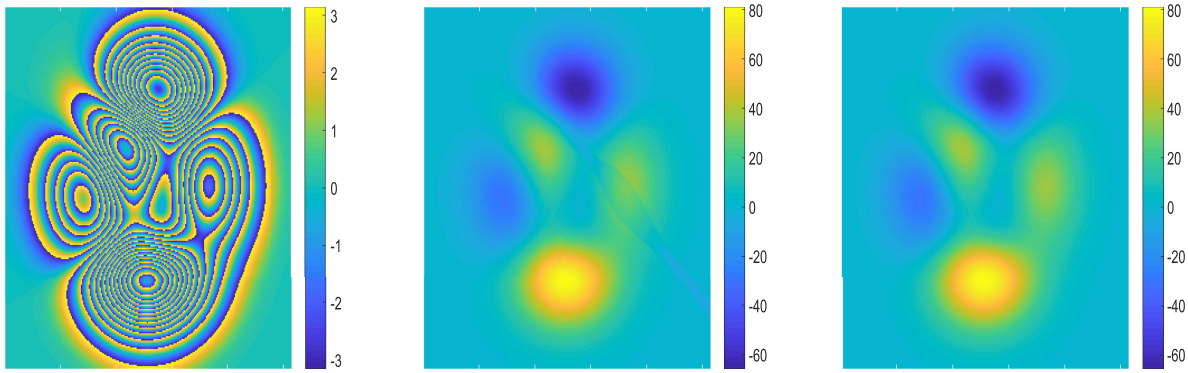

(a) (b) (c)

Fig. 2. Unwrapped images using CKFPU and SCKFPU on a sequential path-following strategy.

TABLE III
CPU TIME (S) COMPARISON

EKFPU	UKFPU	CKFPU	SCKFPU
2.4873	5.9394	7.4501	6.2453

Compared with the unwrapped result obtained by the CKFPU method, the unwrapped image using the SCKFPU method is much better. Fig. 2(b) shows incorrect unwrapping result using the CKFPU method, whereas Fig. 2(c) shows the correct and superior unwrapping result using the SCKF method. The reason why the unwrapping performance of the CKFPU method is degraded is that we cannot randomly select the parameter to meet the requirement of the symmetry and positive definiteness of an error covariance matrix. Assume that the simulation is implemented using MATLAB 7.14.0 (R2017a) on an HP PC with eight-core CPU of Intel (R) Core (TM) i7-4790 3.60 GHz. CPU time comparison of the methods is given in Table III.

Although the unwrapping performance of the SCKFPU method is the best, the CPU time consumed by it is the third least of all the methods.

In the second scenario, we unwrap the Gaussian shaped surface using the SCKFPU method on sequential path-following and optimal path-following strategies. The Gaussian elevation with InSAR noise is generated randomly by a constant coherence of 0.90 [37]. The Gaussian shaped surface is generated by function '$f(x,y) = \text{top} \cdot \exp(-\frac{x^2}{2\sigma_x^2} - \frac{y^2}{2\sigma_y^2})$', where top is set as 7π, and the standard deviations σ_x and σ_y along x- and y-axis are set as 10 and 15, respectively. The value of the adjustable weight r is set as 1.8. The original wrapped phases, the unwrapped phases, and the wrapped difference phases are shown in Fig. 3.

The unwrapping performance of the SCKFPU method on an optimal path-following strategy is much better than that on a sequential strategy. From their unwrapped images, the SCKFPU method on a sequential path-following strategy can cause severe error propagation and leads to the final failure to the unwrapped image, while the SCKFPU method on an optimal path-following strategy can circumvent the problem of error propagation and obtain the final unwrapped image with substantially improved unwrapping performance. In addition, from their wrapped difference images, the distribution of residuals and noises using the SCKFPU on an optimal path-following strategy is almost homogeneous and without fringes, which further indicates the correct unwrapped result. On the other hand, the unwrapping result of the SCKFPU on a sequential strategy is incorrect due to the nonhomogeneous distribution of residuals and noises.

In the following, we exploit the unwrapping performance related to the adjustable weight. The Gaussian elevation with InSAR noise generated by a constant coherence of 0.95 is generated randomly. The Gaussian shaped surface is generated by the function '$f(x,y) = \text{top} \cdot \exp(-\frac{x^2}{2\sigma_x^2} - \frac{y^2}{2\sigma_y^2})$', where top is set as 8π, and the standard deviations σ_x and σ_y along x-axis and y-axis are set as 10 and 15, respectively. We simulate the effect of the adjustable weight r on the unwrapping performance using the SCFK method on an optimal path-following strategy. Suppose the values of the adjustable weight r are set as 1.2, 1.9, and 2.5, respectively, the unwrapping results are shown as follows.

From the unwrapped images with $r = 1.5$ and $r = 2.5$ shown in Fig. 4, there exist obvious errors that indicate the incorrect unwrapping results. On the other hand, the unwrapped image with $r = 1.9$ appears much better and illustrates the correct unwrapping result. Moreover, the distribution of the residuals and noises is almost homogeneous in the wrapped difference phases with $r = 1.9$, whereas those with $r = 1.5$ and $r = 2.5$ are not. This further illustrates that the correct unwrapping result can only be achieved with $r = 1.9$. Thereby, it can be concluded that the selection of the adjustable weight r is important and an inappropriate value may yield failure to phase unwrapping.

C. InSAR Data

In the first scenario, we consider the Longs Peak dataset [2]. This true dataset was obtained by using an InSAR simulator that models the SAR point spread function, the InSAR geometry, the speckle noise, and the layover and shadow phenomena. Specifically, the dataset was generated based on a real DEM of mountainous terrain around Longs Peak and Isolation Peak,

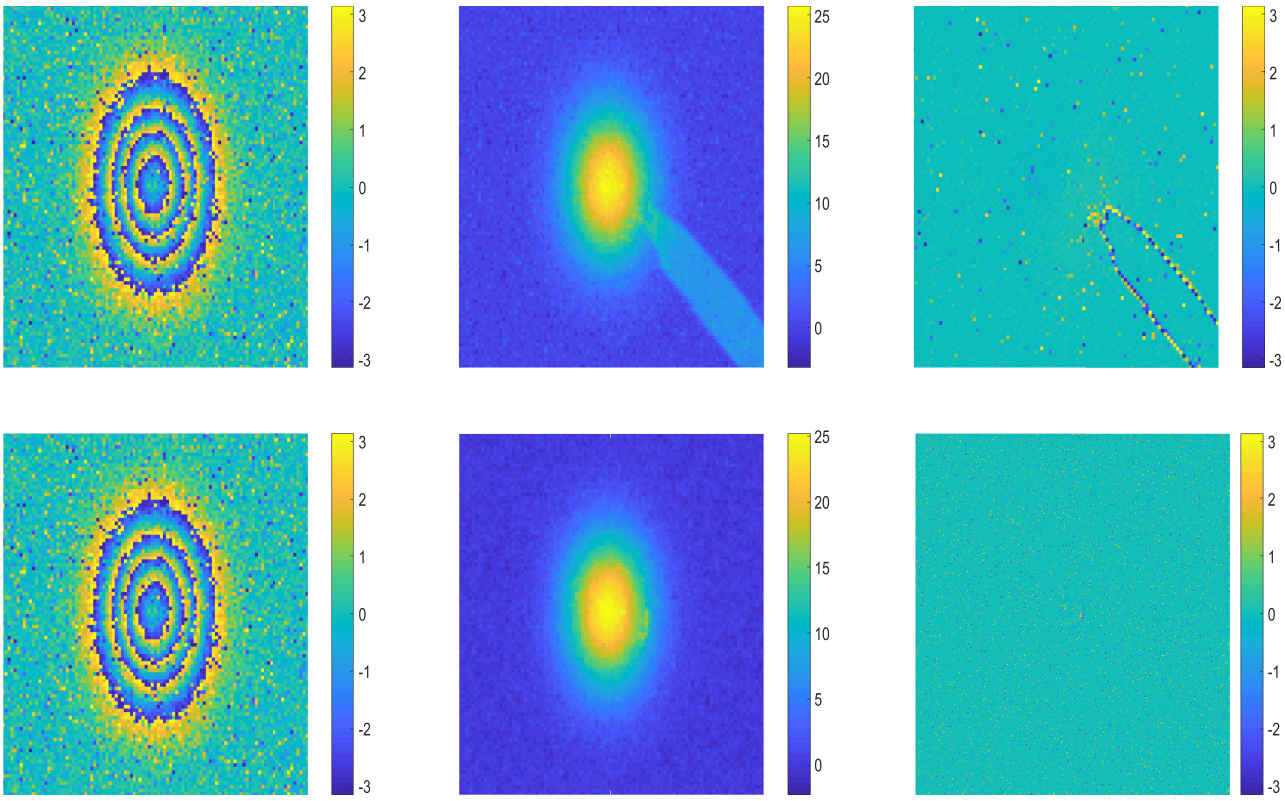

Fig. 3. Unwrapped results using the SCKFPU method on different strategies. Left: original wrapped phases; center: unwrapped phases; right: wrapped difference phases.

TABLE IV
PERFORMANCE ANALYSIS

	Residual counts	MSEs (Wrapped)	NELP
Original	880		
EKFPU	792	0.1635	15687
UKFPU	832	0.1835	15812
CKFPU	791	0.1638	15684
SCKFPU	769	0.1308	15079

TABLE V
RESIDUAL COUNTS AND MSE VALUES FOR THE WRAPPED PHASES

Methods	Residual counts	MSEs(rad^2)
SCKFPU$_1$	743	0.1244
SCKFPU$_2$	837	0.1432

CO, USA, using a high-fidelity InSAR simulator. The value of the adjustable weight r is set as 1.8.

The wrapped images, the unwrapped images, and the different wrapped images are shown in Fig. 5.

The residual counts of the original wrapped phases and the rewrapped phases, the MSE values for the wrapped phases, and NELP are listed in Table IV. From Fig. 5, though the unwrapped images of all the unwrapping methods look similar, the unwrapping performance of the SCKFPU is a bit better. Specifically, the noise in the ellipsoidal region in difference interferometric phase of the SCKFPU method is much smaller than that using other unwrapping methods. The same results can also be obtained from Table IV. It has not only the smallest MSE value, but also the least residual counts. In addition, the SCKFPU has the least NELP, which means this unwrapping algorithm preserves the discontinuity best. The reason why the performance of the EKFPU and UKFPU is not satisfying lies in the complexity and nonlinearity of InSAR phase unwrapping problem. In addition, the CKFPU method has the worst performance due to the constraint on the selection of parameters.

In the following, we unwrap the Longs Peak dataset using different optimal phase estimate functions—one is our designed function (37), and the other is (10) in [21]. The corresponding SCKFPU methods are termed SCKFPU$_1$ and SCKFPU$_2$. The value of the adjustable weight is set as 2.2. The wrapped images, the unwrapped images, and the difference interferometric images are shown as follows. The residual counts of the rewrapped phases and the MSE values for the wrapped phases are listed in Table V. Compared with the SCKPU method using phase quality estimate function (10) in [21], the unwrapping performance of the SCKPU method using our designed phase quality estimate function is a little bit better, which has both less residual count and smaller MSE value though their unwrapping images look similar.

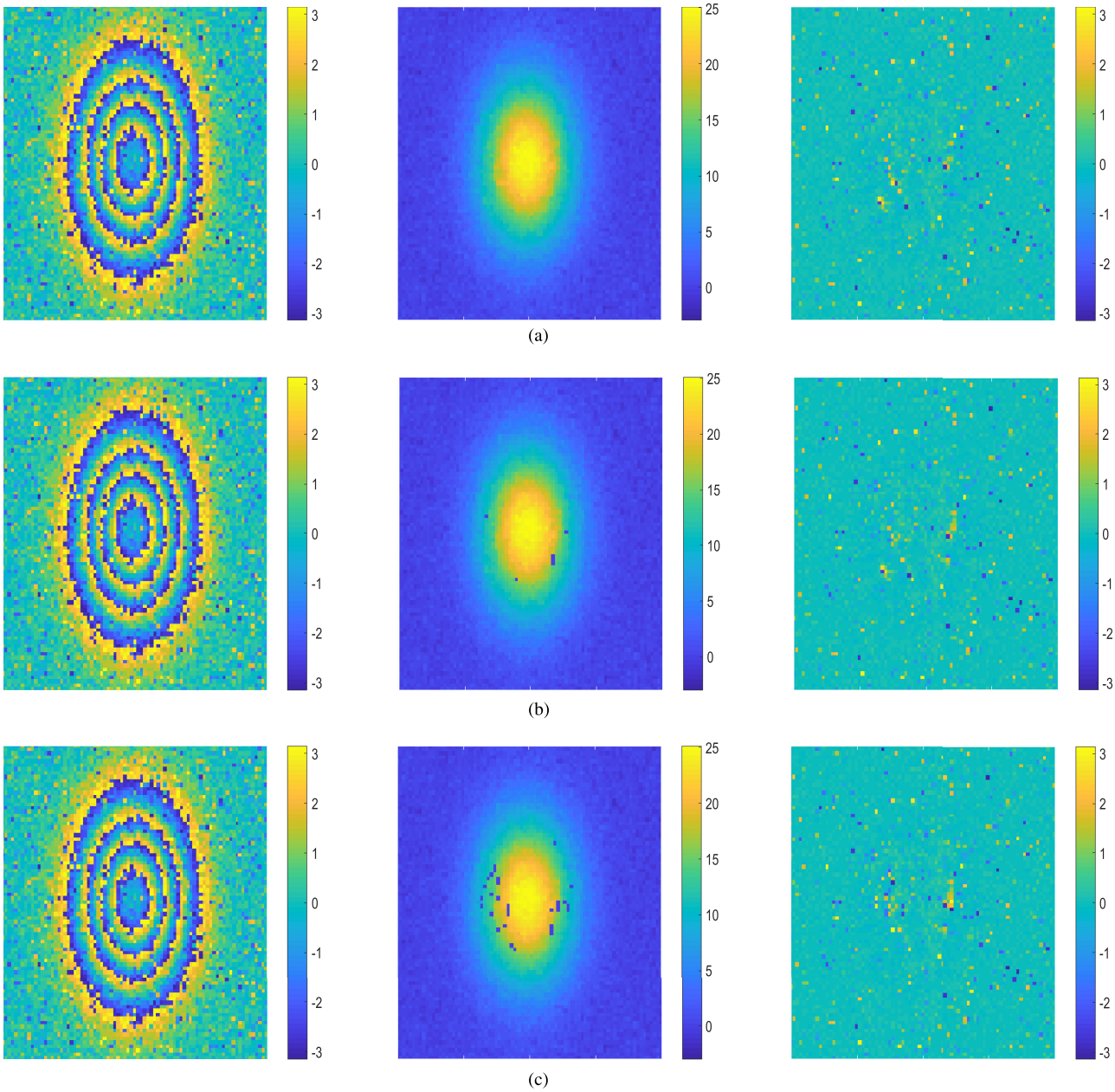

Fig. 4. Unwrapping effect—the adjustable weight. Left: wrapped phases; center: unwrapped phases; right: wrapped difference phases. (a) $r = 1.2$. (b) $r = 1.9$. (c) $r = 2.5$.

In the second scenario, we consider the dataset based on TerraSAR-X/TanDEM-X formation satellite InSAR image pairs. The dataset corresponds to an irradiation area from Xi'an and the Qinling mountain, China. The master and slave images were acquired by Terra SAR-X/TanDEM-X on November 16, 2015. Their working mode is strip and full polarization mode. The dataset is from HH polarization channel, whose absolute orbit number is 45 928, observation mode is down-orbit, distance resolution is 1.00 m, and azimuth resolution is 6.60 m. This dataset is quite challenging as it can be perceived from the low values of the estimated coherence shown in the right-hand side of Fig. 7 and from the highly noisy interferometric phase shown in the left-hand side of Fig. 8. We compare the performance of the unwrapping methods EKFPU, UKFPU, CKFPU, and SCKFPU on an optimal path-following strategy. The value of the adjustable weight is set as 2.2. The original images, the unwrapped images, and the wrapped difference phases are shown in Fig. 8.

The number of the original wrapped phase is 12 449. The residual counts of the rewrapped phases are listed in Table VI.

From the wrapped difference phases shown in Fig. 8, though there are no fringes in the wrapped difference images for all the unwrapping methods, the distribution of the residuals and noises using SCKFPU on an optimal path-following strategy is a little bit more homogeneous than that using other methods. From Table VI, the SCKFPU has both the least residual count and the best SNR value of the rewrapped image, which means

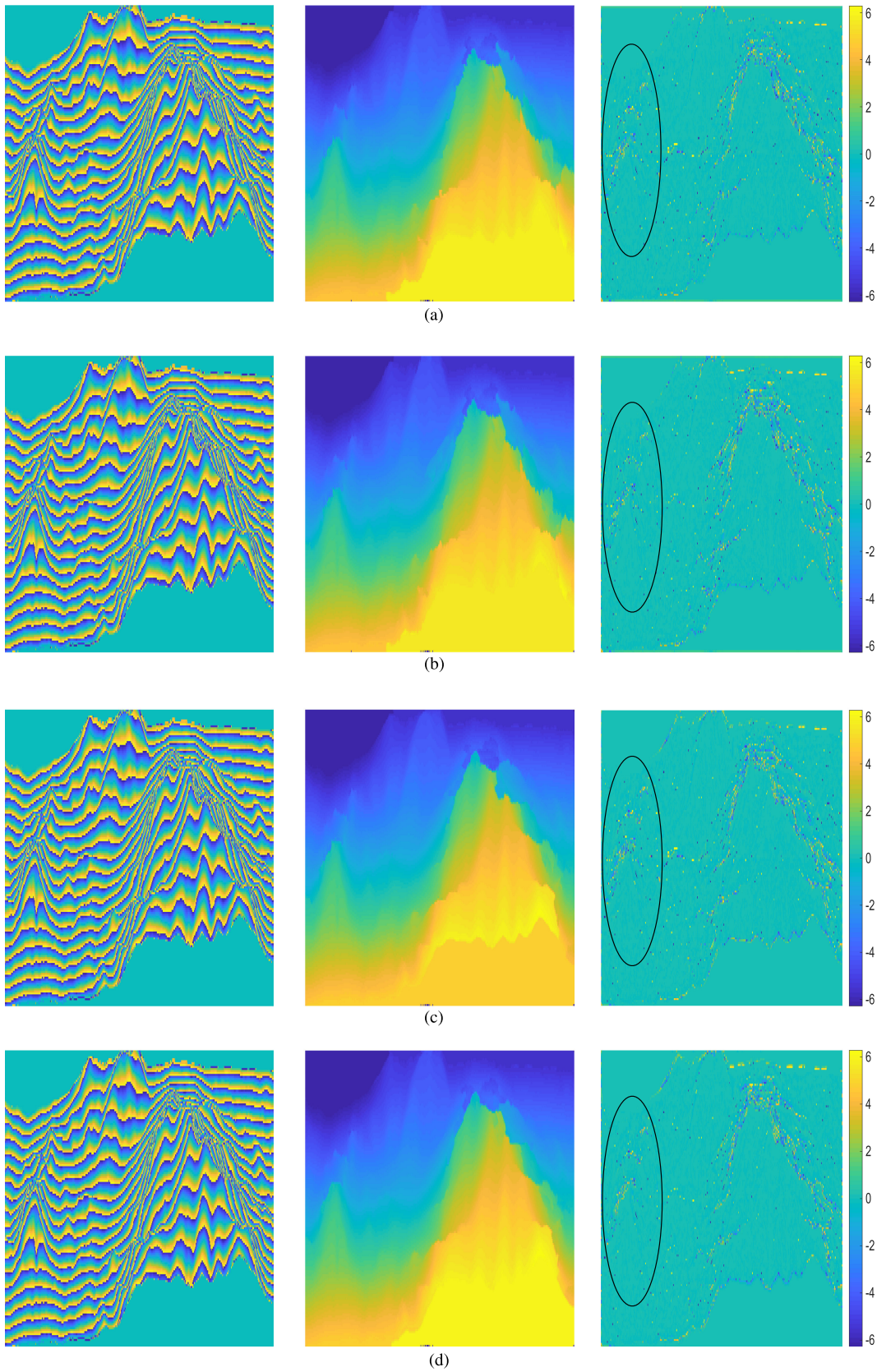

Fig. 5. Unwrapping results using EKFPU, UKFPU, CKFPU, and SCKFPU methods on an optimal path-following strategy. Left: wrapped phases; center: unwrapped phases; right: difference interferometric phases. (a) EKFPU. (b) UKFPU. (c) CKFPU. (d) SCKFPU.

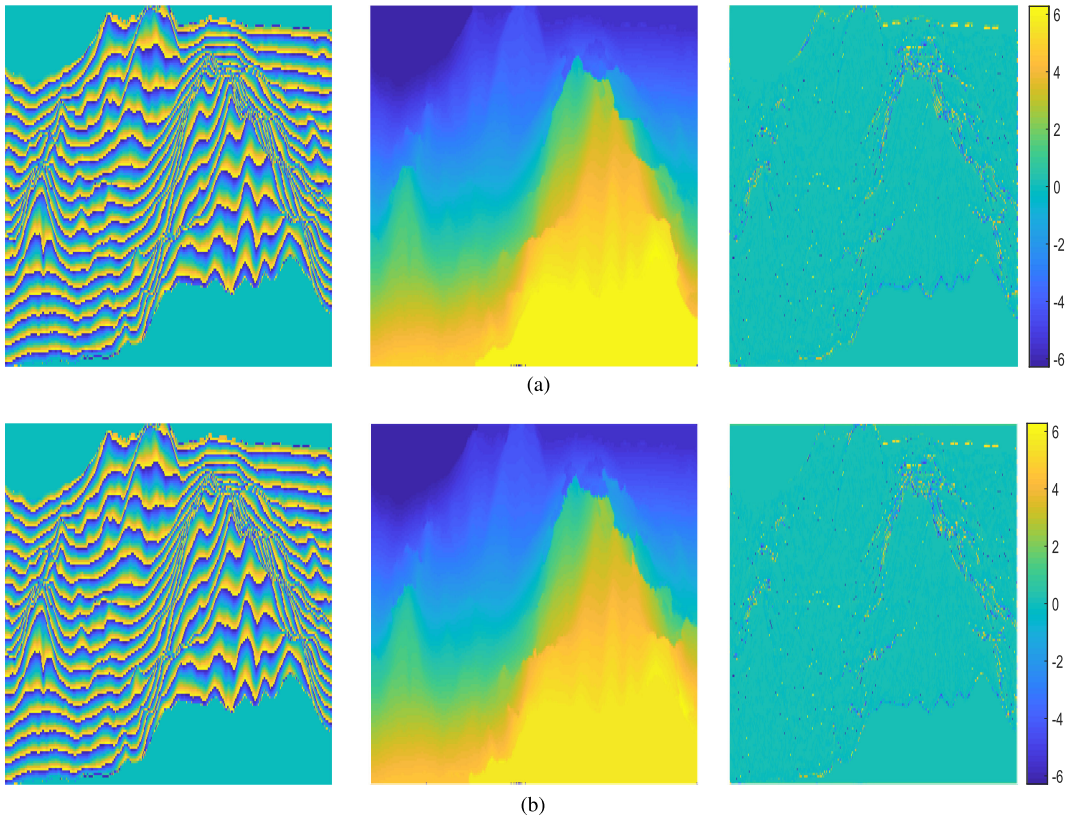

Fig. 6. Unwrapping results using SCKFPU methods on (37) and (10) in [21]. Left: wrapped phases; center: unwrapped phases; right: difference interferometric phases. (a) SCKFPU_1. (b) SCKFPU_2.

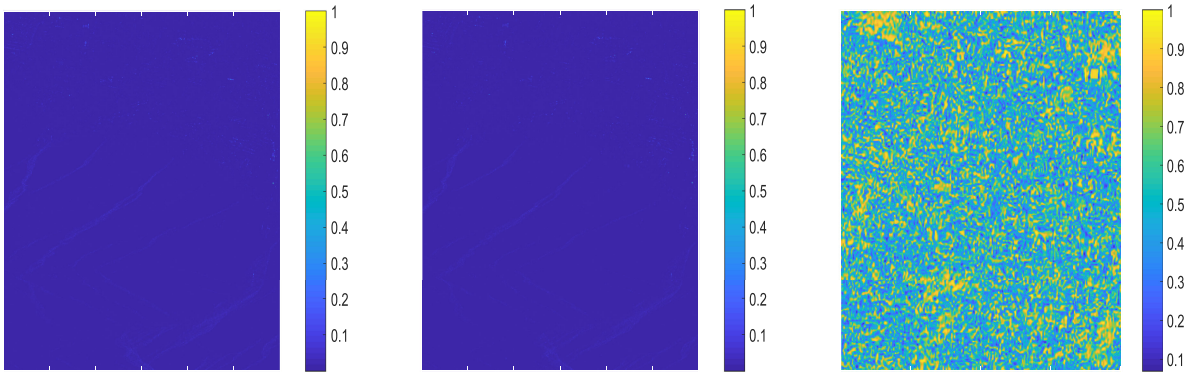

Fig. 7. TerraSAR-X/TanDEM-X dataset. Left: normalized amplitude of master SAR image; center: normalized amplitude of slave SAR image; right: coherence.

TABLE VI
RESIDUAL COUNTS AND SNR

Methods	Residual counts	SNR(dB)
$EKFPU_1$	8930	6.6405
$UKFPU_2$	9296	6.6403
$CKFPU_2$	8926	6.6406
$SCKFPU_2$	8375	8.5172

its noise reduction performance is the best. Thereby, it can be concluded that the unwrapping performance of SCKFPU on an optimal path-following strategy is the best.

In the following, we unwrap this dataset using the SCKFPU method on an optimal path-following strategy based on coherence and our designed function (37), respectively. The corresponding SCKFPU methods are termed $SCKFPU_{op}$ and $SCKFPU_{co}$, respectively. Suppose that the value of the adjustable weight is set as 2.3 and the original wrapped images, the unwrapped images, and the wrapped difference phases are shown as follows.

The number of the original wrapped phase is 12 449. The residual counts of the rewrapped phases and the corresponding SNR of the unwrapped phases using the $SCKFPU_{op}$ and the $SCKFPU_{co}$ are listed in Table VII.

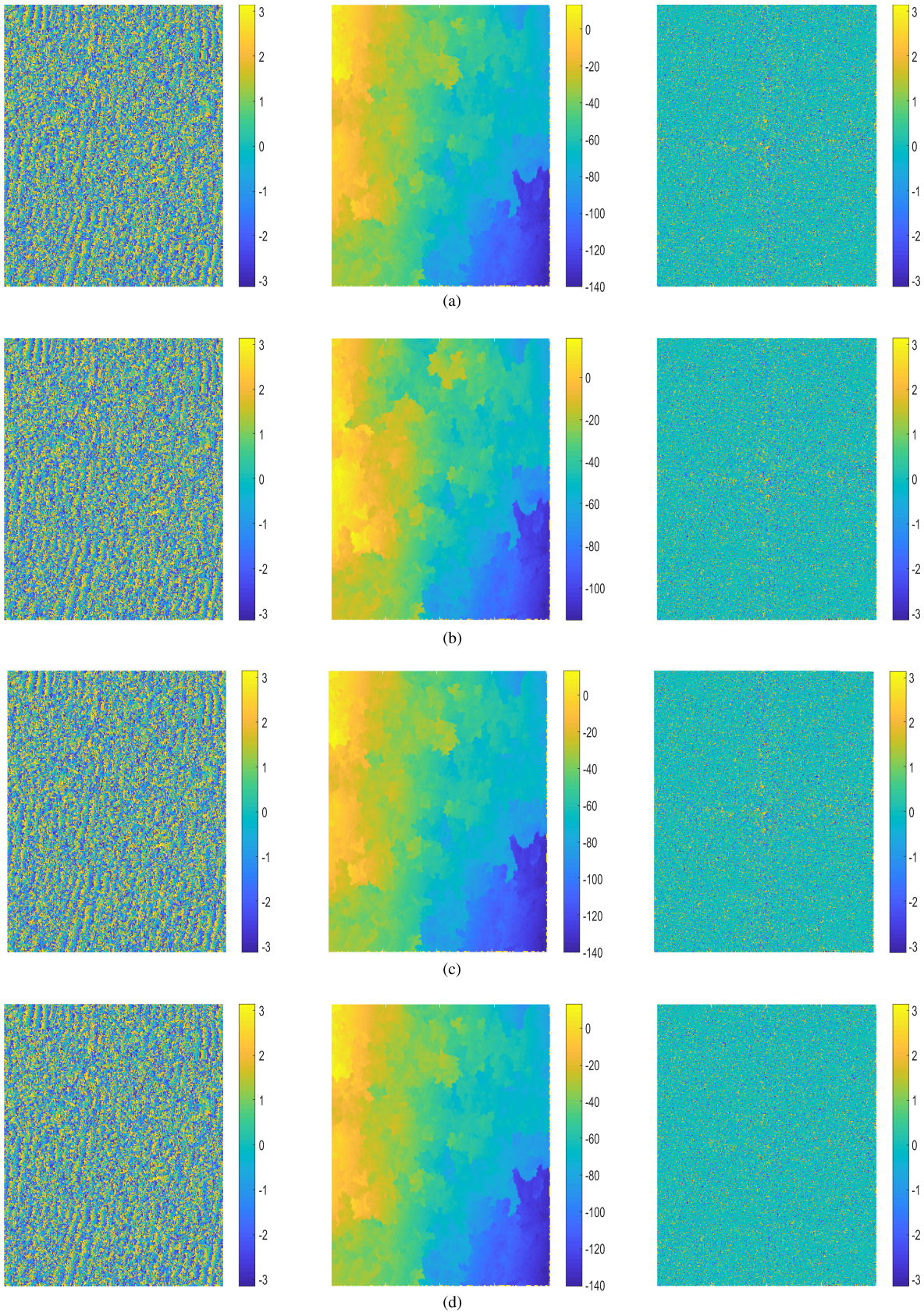

Fig. 8. Unwrapping results. Left: original wrapped phases; center: unwrapped phases; right: wrapped difference phases. (a) EKFPU. (b) UKFPU. (c) CKFPU. (d) SCKFPU.

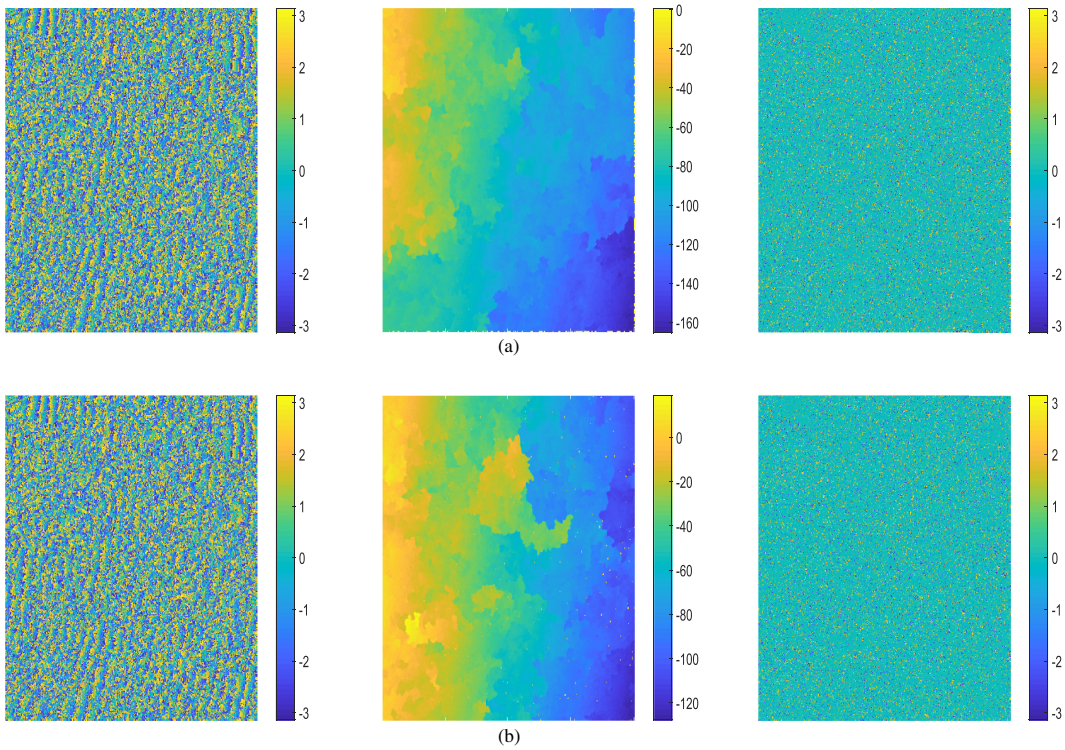

Fig. 9. Unwrapping results based on $\text{SCKFPU}_{\text{op}}$ and $\text{SCKFPU}_{\text{co}}$ methods. Left: original wrapped phases; center: unwrapped phases; right: wrapped difference phases. (a) $\text{SCKFPU}_{\text{op}}$. (b) $\text{SCKFPU}_{\text{co}}$.

TABLE VII
RESIDUAL COUNTS AND SNR

Methods	Residual counts	SNR(dB)
$\text{SCKFPU}_{\text{op}}$	8361	9.0716
$\text{SCKFPU}_{\text{co}}$	8414	3.0340

From the unwrapped images, we can see the color changes of some pixels using the $\text{SCKFPU}_{\text{co}}$ method are abrupt while those of the whole image using the $\text{SCKFPU}_{\text{op}}$ method are continuous, which indicates that the SCKFPU method on (37) yields less structured error and smaller bias. In addition, from their wrapped difference images, both methods have the correct unwrapped results. However, the distribution of the residuals and noises on (37) is a little bit more homogeneous than that on coherence. From Table VII, the $\text{SCKFPU}_{\text{op}}$ has less residual count and much higher SNR value as compared with the $\text{SCKFPU}_{\text{co}}$. Thereby, it can be concluded that the unwrapping performance of the $\text{SCKFPU}_{\text{op}}$ method on an optimal path-following strategy using (37) is better compared with that using coherence alone.

V. CONCLUSION

In this article, we present a novel phase unwrapping method termed the SCKFPU method. Specifically, as the system model of the InSAR phase unwrapping can be formulated as the MJS for tracking a maneuvering target, we propose the SCKFPU method based on the SCKF. Moreover, a phase quality estimate function is designed and an optimal path-following strategy is proposed. From the simulations, the unwrapping performance of the SCKFPU method is the best of all the unwrapping methods based on the tracking filters, though the running time is not the least. It can not only unwrap the phase efficiently, but also can suppress the noises, eliminate the residuals, and preserve the fringe continuity effectively.

ACKNOWLEDGMENT

The authors would like to thank Prof. Z.-Q. (Tom) Luo of the Chinese University of Hongkong (Shenzhen) for his helpful suggestions.

REFERENCES

[1] E. Rodrigues and J. Martin, "Theory and design of interferometric synthetic aperture radars," *IEE Proc.-F*, vol. 139, no. 2, pp. 147–159, 1992.
[2] D. C. Ghiglia and M. D. Pritt, *Two Dimensional Phase Unwrapping: Theory, Algorithms, and Software*. Hoboken, NJ, USA: Wiley, 1998.
[3] R. M. Goldstein, H. A. Zebker, and C. L. Werner, "Satellite radar interferometry: Two dimensional phase unwrapping," *Radio Sci.*, vol. 23, no. 4, pp. 713–720, 1988.
[4] E. Trouve, J.-M. Nioclas, and H. Maitre, "Improving phase unwrapping techniques by the use of local frequency estimates," *IEEE Trans. Geosci. Remote Sens.*, vol. 36, no. 6, pp. 1963–1972, Nov. 1998.
[5] R. Jiang, D. Y. Zhu, and Z. D. Zhu, "Phase unwrapping approach using equivalent residues for InSAR," *J. Nanjing Univ. Aero. Astronaut.*, vol. 45, no. 2, pp. 209–216, 2013.
[6] H. W. Yu, Z. F. Li, and Z. Bao, "Residues cluster-based segmentation and outlier-detection method for large-scale phase unwrapping," *IEEE Trans. Image Process.*, vol. 20, no. 10, pp. 2865–2875, Oct. 2011.
[7] W. Xu and I. Cumming, "A region growing algorithm for InSAR phase unwrapping," in *Proc. Int. Geosci. Remote Sens. Symp.*, vol. 4, pp. 2044–2046, 1996.

[8] K. Kun and Z. B. Zhang, "A region growing phase unwrapping approach combining local frequency estimation for InSAR," *Electronic. Sci. Tech.*, vol. 23, no. 4, pp. 69–72, 2010.
[9] H. Takajo and T. Takahashi, "Least-squares phase estimation from the phase differences," *J. Opt. Soc. Amer. A*, vol. 5, no. 3, pp. 416–425, 1988.
[10] M. D. Pritt and J. S. Shipman, "Least-squares two-dimensional phase unwrapping using FFT's," *IEEE Trans. Geosci. Remote Sens.*, vol. 32, no. 3, pp. 706–708, May 1994.
[11] X. P. Wang, "Minimum cost flow and its ameliorative algorithm for phase unwrapping of InSAR image," *Sci. Surveying Mapping*, vol. 35, no. 4, pp. 129–131, 2010.
[12] M. Costantini, "A novel phase unwrapping method based on network programming," *IEEE Trans. Geosci. Remote Sens.*, vol. 36, no. 3, pp. 813–821, May 1998.
[13] H. S. Srivastava, P. Patel, and R. R. Navalgund, "Detection and density mapping of forested areas using SAR interferometry technique," *Int. J. Geoinformat.*, vol. 3, no. 2, pp. 1–10, 2007.
[14] L. Pulvirenti, M. Chini, N. Pierdicca, and G. Boni, "Use of SAR data for detecting floodwater in urban and agricultural areas: The role of the interferometric coherence," *IEEE Trans. Geosci. Remote Sens.*, vol. 54, no. 3, pp. 1532–1544, Mar. 2016.
[15] V. Kumar and G. Venkataraman, "SAR interferometric coherence analysis for snow cover mapping in the western Himalayan region," *Int. J. Digit. Earth*, vol. 4, no. 1, pp. 78–90, 2011.
[16] J. J. Xiao, Z. Q. Luo, and M. Jiang, "Two-dimensional phase unwrapping using semidefinite relaxation," in *Proc. IEEE Int. Conf. Acoust., Speech Signal Process.*, 2009, pp. 1105–1108.
[17] Z. Q. Luo, W. K. Ma, A. M.-C. So, Y. Y. Ye, and S. Z. Zhang, "Semidefinite relaxation of quadratic optimization problems," *IEEE Signal Process. Mag.*, vol. 27, no. 3, pp. 20–34, May 2010.
[18] B. Ristic *et al.*, *Beyond the Kalman Filter: Particle Filters for Tracking Applications*. Norwood, MA, USA: Artech House, 2004.
[19] O. Loffeld, H. Nies, S. Y. Knedlik, and Y. Wang, "Phase unwrapping for SAR Interferometry-a data fusion approach by Kalman filtering," *IEEE Trans. Geosci. Remote Sens.*, vol. 46, no. 1, pp. 47–58, Jan. 2008.
[20] J. J. Martinez-Espla, T. Martinez-Marin, and J. M. Lopez-Sanchez, "A particle filter approach for InSAR phase filtering and unwrapping," *IEEE Trans. Geosci. Remote Sens.*, vol. 47, no. 4, pp. 1197–1211, Apr. 2009.
[21] X. M. Xie, "Enhanced multi-baseline unscented Kalman filtering phase unwrapping algorithm," *J. Syst. Eng. Electron.*, vol. 27, no. 2, pp. 343–351, 2016.
[22] W. L. Liu, Z. F. Bian, Z. G. Liu, and Q. Z. Zhang, "Evaluation of a cubature Kalman filtering-based phase unwrapping method of differential interferograms with high noise in coal mining areas," *Sensors*, vol. 15, pp. 16336–16357, 2015.
[23] A. Ienkaran and H. K. Simon, "Cubature Kalman filters," *IEEE Trans. Autom. Control*, vol. 54, no. 6, pp. 1254–1269, Jun. 2009.
[24] X. M. Luo, X. F. Wang, Y. H. Wang, and S. Q. Zhu, "Efficient InSAR phase noise reduction via compressive sensing in the complex domain," *IEEE J. Sel. Topics Appl. Earth Observ.*, vol. 11, no. 5, pp. 1615–1632, May 2018.
[25] O. Loffeld and C. Amdt, "Estimating the derivative of modulo-mapped phases," in *Proc. Int. Conf. Acoust., Speech, Signal Process.*, 1997, vol. 4, pp. 1–10.
[26] S. Boyd and L. Vandenberghe, *Convex Optimization*. Cambridge, U.K.: Cambridge Univ. Press, 2004.
[27] E. Trouve, "Fringe detection in noisy complex interferograms," *Appl. Opt.*, vol. 35, no. 20, pp. 3799–3806, 1997.
[28] S. N. Madsen, "Estimating the Doppler centroid of SAR data," *IEEE Trans. Aerosp. Electron. Syst.*, vol. 25, no. 2, pp. 134–140, Mar. 1989.
[29] X. M. Luo, B. Jiu, S. D. Chen, and Q. B. Ge, "ML estimation of transition probabilities for an unknown maneuvering emitter tracking," *Signal Process.*, vol. 105, pp. 248–260, 2016.
[30] M. K. Steven, *Fundamentals of Statistical Signal Processing. Volume I: Estinimation Theory.* Englewood Cliffs, NJ, USA: Prentice-Hall, 1998.
[31] U. Spagnolini, "2-D phase unwrapping and instantaneous frequency estimation," *IEEE Trans. Geosci. Remote Sens.*, vol. 36, no. 3, pp. 813–821, May 1995.
[32] R. M. Goldenstein and C. L. Radar, "Radar interferogram filtering for geophysical applications," *Geophys. Res. Lett.*, vol. 25, no. 21, pp. 4035–4038, 1998.
[33] B. Cai, D. Liang, and Z. Dong, "A new adaptive multiresolution noise-filtering approach for SAR interferometric phase images," *IEEE Geosci. Rem. Sens. Lett.*, vol. 5, no. 2, pp. 266–270, Apr. 2008.
[34] G. Valadão and J. M. Bioucas-Dias, "CAPE: Combinatorial absolute phase estimation," *J. Opt. Soc. Amer. A*, vol. 26, no. 9, pp. 2093–2106, 2009.
[35] Y. Yan *et al.*, "Coseismic slip distribution of the 2005 Kashmir earthquake from SAR amplitude image correlation and differential interferometry," *Geophys. J. Int.*, vol. 193, no. 1, pp. 29–46, 2013.
[36] H. X. Hao, J. M. Bioucas-Dias, and V. Katkovnik, "Interferometric phase image estimation via sparse coding in the complex domain," *IEEE Trans. Geosci. Remote Sens.*, vol. 53, no. 5, pp. 2587–2602, May 2015.
[37] J. Dias and J. Leitão, "The Z/spl pi/M algorithm for interferometric image reconstruction in SAR/SAS," *IEEE Trans. Image Process.*, vol. 11, no. 4, pp. 408–422, Apr. 2002.

Xiaomei Luo received the B.S. degree in industrial enterprise automation from Nanchang University, Jiangxi, China, in 1994, and the Ph.D. degree in communications and information system with the School of Telecommunication Engineering from Xidian University, Xian, China, in 2015.

She is currently a Vice Professor with the School of Information Engineering, Nanchang University, Jiangxi, China. Her current research interests include wireless communications, localization, tracking and detection in wireless sensor network, and microwave remote sensing processing.

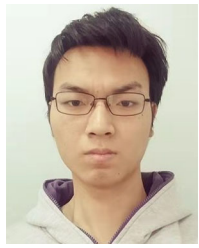

Hongtao Li received the B.S. degree in communication engineering from Nanchang University, Jiangxi, China, in 2018. He is currently a candidate M. S. student in electronics and communication engineering from the School of Information Engineering, Nangchang University, Jiangxi, China.

His current research interests include wireless communications and microwave remote sensing data processing.

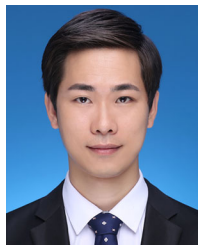

Zhilong Dong received the B.Sc. degree in information and computational science from Beihang University, Beijing, China, in 2012, and the Ph.D. degree in computational mathematics from University of Chinese Academy of Sciences, Beijing, China, in 2017.

He is currently working as an Assistant Professor with Xi'an Jiaotong University. His research interests include nonlinear optimization, sparse optimization, applications in wireless communication, and financial engineering.

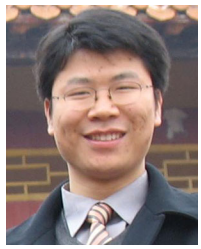

Shengqi Zhu received the B.S. degree in electrical engineering from Xidian University, Xi'an, China, in 2005. He is currently working toward the Ph.D. degree in radar signal processing from the National Key Laboratory of Radar Signal Processing, Xidian University.

His current work includes synthetic aperture radar (SAR) Doppler parameter estimation, space-time adaptive processing (STAP), SAR ground moving target indication (GMTI), bistatic STAP algorithms, and robust array signal processing. He has also worked on systems for processing real airborne SAR data and designed the SAR/GMTI algorithms for the distributed small satellite SAR systems in China.